Performance analysis of P-SnS thin films fabricated using CBD technique for photo detector applications

P. Sateesh[a,*], A. Raveendra[b,*], M. Ashok[c], S.S. Sivaraju[d], K. Umadevi[e], N. Rajeswaran[f]

[a]*Department of Physics, St.Peter'S Engineering College, Hyderabad,T.S, 500100, India*

[b]*Department of Mechanical Engineering, Malla Reddy Engineering College, Hyderabad,T.S, 500100, India*

[c]*Department of CSE, Malla Reddy Institute of Engineering and Technology, Hyderabad, T.S, 500100, India*

[d]*Department of EEE, RVS College of Engineering and Technology, Coimbatore, T.N, 641402, India*

[e]*Department of H&S, Gokaraju Rangaraju Institute of Engineering and Technology, Hyderabad, TS,500090, India*

[f]*Department of EEE, Malla Reddy College of Engineering ,Hyderabad, T.S, 500100, India*

In the present work, SnS thin films were prepared using the CBD technique at room temperature and varying annealing temperaturesfrom300 to 450 °C for photo detector applications. The prepared samples were characterized using different techniques for analyzing the structural, optical, morphological, and photo sensing properties of the samples. From XRD analysis, the diffraction pattern of all the prepared thin films shows the pristine SnS phase of the samples possessing an orthorhombic phase without the presence of any impurity phases. Among the fabricated thin films, the SnS thin film annealed at a temperature of 350 °C reveals the highest crystallite size. The Raman results showed the vibrational modes of SnS films and with the increase in growth temperature, the peaks are slightly shifted towards the lower wavelength region. Morphological results show that the SnS thin films exhibit a uniform morphology of 2-D petal-like morphology with different sizes. The UV-vis spectroscopic study shows the decrease in the bandgap value of the samples with the increase in annealing temperature. The photo sensing properties of the fabricated samples show the SnS sample annealed at 400 °C has a higherresponsivityvalueof6.40×$10^{-2}$$AW^{-1}$,externalquantumefficiency(EQE)valueof14.9%, and the detectivity value of 6.05 × 10^{9} Jones. Finally, the transient photo response results suggest that the SnS annealed at 350 °C shows a rise and fall time of 1.5 and 2.5 s compared to the othersampleswhichwouldbebettersuitedforphotodetectorapplications. The electrical conductivity and photo-conductivity of the films increase by more than two orders with increase of film thickness from 170 nm to 915 nm. Hall Effect measurements confirm the p-type nature of the as-prepared SnS thin films.

(Received August 9, 2023; Accepted November 2, 2023)

Keywords: SnS thin films, CBD, Photo detector, EQE, Band gap, UV-vis, Hall Effect.

1. Introduction

The IV–VI groups of semiconductors have been attracting much interest due to their potential application in optoelectronic devices and solar cells. Dittrichet al[1], have studied sulfosalts and emphasized their importance in the field of optoelectronics [2]. In recent years, tin chalcogenide compounds such as SnS, SnS_2 [3] and Sn_2S_3 [4] have a significant role to play in the fabrication of photovoltaic devices because of its favorable optical band gap energy, high optical transmittance, and optical absorption coefficient. These semiconductor thin films are made up of

* Corresponding author: satheesh.nanofilms@gmail.com
https://doi.org/10.15251/CL.2023.2011.779

inexpensive, non-toxic and earth abundant constituents [4]. The optoelectronic properties of Sn–S based compounds are suitable for building photovoltaic p–n or p–i–n structures with high conversion efficiency of the order of 25% [5]. Among the tin chalcogenides, tin mono sulfide (SnS) is a very promising material for the fabrication of optoelectronic devices because of its favorable optical band gap energy of 1.35 eV, near optimum for photovoltaic solar energy conversion and high optical absorption coefficient> 10^4 cm^{-1} [2]. For p–n hetero junction devices using p-type SnS as the absorber layer with wide energy band gap transparent semiconductor as the n-type partner[6].Sno_2, Zno,Cds and ZnS are the best choice for n-type material with p-type SnS layer for hetero junction devices. In general, the physical properties of a material, particularly in thin film form depend on deposition parameters as well as on the film thickness. The performance of the hetero junction depends up on the thickness of n-type partner and various properties of deposited SnS films SnS_2 and Sn_2S_3 have been used for many applications such as window layers [3]. and near lattice matched hetero junctions[4]. in thin film solar cells because of their suitable optical and electrical properties. SnS thin films have been prepared using different methods such as vacuum thermal evaporation[6],Co-evaporation[7] ,radio frequency sputtering[8], electron beam evaporation[9], atomic layer deposition[10], Pulse electro deposition[11], Plasma enhanced chemical vapor deposition[12],Spray pyrolysis[13-15] chemical bath deposition[16-17], Sol-gel process[18], and electrochemical deposition[19].

In the present work, the SnS thin films have been deposited on sapphire substrates with different thicknesses from 120 nm to 930 nm by CBD technique. The structural, surface morphological, electrical and optical properties of these films have been investigated as a function of the film thickness. The influence of thickness on photo conductivity, photo response, and decay time of the films is calculated and reported here. The optical properties such as refractive index n (λ), extinction coefficient k (λ), absorption coefficient (α) and band gap (Eg) of the deposited films studied and reported using the interference phenomena in transmission spectra data.

In the present work, SnS thin films were prepared using the Chemical bath deposition Technique at room temperature and varying annealing temperatures from 200 to 350 °C for photo detector applications. The prepared samples were characterized using different techniques for analyzing the structural, optical, morphological, and photo sensing properties of the samples. From XRD analysis, the diffraction pattern of all the prepared thin films shows the pristine SnS phase of the samples possessing an orthorhombic phase without the presence of any impurity phases. Among the fabricated thin films, the SnS thin film annealed at a temperature of 300 °C reveals the highest crystallite size [20-21]. The Raman results showed the vibrational modes of SnS films and with the increase in growth temperature, the peaks are slightly shifted towards the lower wavelength region. Morphological results show that the SnS thin films exhibit a uniform morphology of 2-D petal-like morphology with different sizes[22-23]. The UV-vis spectroscopic study shows the decrease in the bandgap value of the samples with the increase in annealing temperature. The photo sensing properties of the fabricated samples show the SnS sample annealed at 300 °C has a higher responsivity value of 6.40×10^{-2} AW^{-1}, external quantum efficiency (EQE) value of 14.9%[24], and the detectivity value of 6.05×10^9 Jones. Finally, the transient photoresponse results suggest that the SnS annealed at 300 °C shows a rise and fall time of 1.5 and 2.5 s compared to the other samples which would be better suited for photo detector applications [26].

2. Experimental

Tin sulfide (SnS) thin films have been deposited on glass substrates in the thickness range of 170 nm to 915 nm using Chemical bath deposition Technique. In this study specified amount of stannous chloride (sigma-Aldrich, 99.999%) was weighed into a100ml beaker in order to prepare various concentrations of $SnCl_2$ solution (0.1, 0.3&0.5M). Then about 2ml of glacial acetic acid was added to dissolve the stannous chloride taken in a beaker and heated at 410k with stirring for 10 min on a hot plate followed by the addition of 1ml of HCL resulting in a clear transparent solution to a 100ml beaker. After that 30ml triethanolamine ($C\ 6H_{15}No_3$) (as supplied diluted to 50%) 16 ml ammonia (NH4OH), 10ml thioacetamide (TA)(0.1M,0.3&0.5M) of experimental

design was added in to the same beaker and the mixture solutions were again stirred. Among this experiment ammonia was added to change the PH in to certain values (PH 9.20, 9.19&8.76) using PH meter. Later the solution poured into another beaker containing clean glass substrate, clamped vertically. The deposition is made at room temperature, the bath colour leaving a clear red to a permanently chocolate brown. SnS films nucleated on to submerged surfaces, including beaker walls in about 24h for one deposition run. At the end of each deposition run, the layer is rinsed in bid stilled water. The sample was preserved in the desiccators for 2-3days and kept for further analysis.

The structural properties of the deposited films were investigated by RIGAKU ULTIMA III X-ray diffractometer. Raman spectroscopy (Horiba lab RAM HR evolution micro-Raman spectrometer) was carried out to identify the phases present in the SnS thin films. The morphology of the deposited layers was studied using Zeiss Ultra 55 FE-SEM. The elemental composition was analyzed using EDS spectra, recorded using Thermo Scientific ultra dry EDS detector attached to Hitachi 3000s SEM. Atomic force microscopy (AFM-Park NX10) was used to study the morphology and surface roughness of the film. The optical transmittance measurements were carried out using UV Vis-NIR spectrometer (JASCO V-670) in the wavelength range of 200–3000 nm. The photo current and photo response of as deposited samples are characterized under AM 1.5 G spectrum at a constant applied bias 5 V using Keithley (6517) by two probe method at room temperature. The temperature dependent resistance measurement of the deposited films was carried out in the temperature range of 320 to 425 K under a vacuum of 10 $^{-}$2 Torr. Hall Effect measurement in vanderpauw configuration (ECOPIA HMS-5000) was employed for understanding the type, carrier density and mobility.

3. Results and discussion

3.1. Structural properties

The structural properties of the SnS thin films produced under the different experimental conditions were examined by x-ray diffraction (XRD), Raman spectroscopy, and scanning electron microscopy (SEM).

3.2. X-Ray diffraction patterns

The XRD patterns were measured with a Rigaku X-ray diffractometer. Measurements were made using a nickel filter(λ = 1.5406 Å)CuKα radiation of 20°□ 2θ°□ 70°, and 0.02°steps. Figure 2 shows the XRD graphs of the SnS semiconductors: as-deposited, annealed for Different temperatures. Based on(JCPDSPDF Card # 39-0354)., The peaks observed in Fig.(1) and Fig.(2) at 2θ values of 32.85^0, 45.85^0 54.95^0 and 75.75^0 the films had diffraction peaks related to (003),(112),(004), (200),(121),(220), (311),(331),(223), and (312) crystal lattices. These peaks indicate an orthorhombic structure, as shown by many previous studies. The films' half-maximum width (FWHM), D_{hkl}(particle size), δ (dislocation density, line m−2), N (number of crystals per unit surface, 1 m−2), and ε (lattice strain)were calculated using the (121) O peak around 2θ ~ 32.00°in the diffraction pattern. More specifically, the crystallite sizes were calculated from the Scherrer equation:

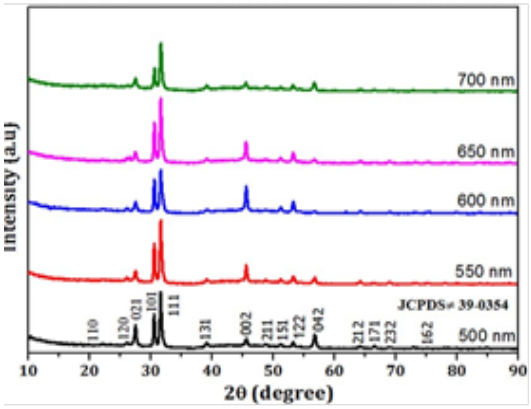

Fig. 1. XRD Spectra of SnS thin films

3.3. Analysis of XRD

Maximum for the film of a thickness of 700nm (seefigure2).Scherer's formula was used to calculate the crystallite size (D) in the deposited films and the equation is presented below (1)

$$D = Kl \div \beta \text{ Cosq} \quad (1)$$

Where β represents the full width at half-maximum of diffraction peak (in radians), λ denotes the wavelength of x-rays, and θ indicates Bragg's angle. The dislocation density was determined by using the equation (2),

$$D = 1 \div n^2 \quad (2)$$

Figure 2shows the relationship between the variations in average crystallite size, DPO, dislocation density, and film thickness. From figure2, it is evident that the crystallite size is initially increased with an increase in thickness, and the highest crystallize size of 38nm is obtained for the sample with a thickness of700nm.Withafurther increase in the thickness, the crystallite size decreased considerably. The dislocation density values showed variations opposite to the crystalline size.

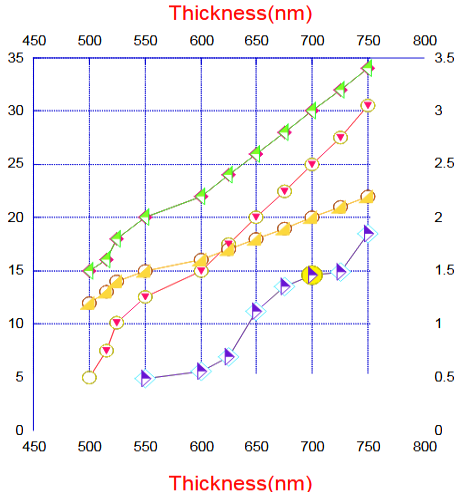

Fig. 2. Variation in average crystallite size, dislocation density, photo current, and degree of preferred orientation(DPO)o the SnS thin films of different thicknesses.

3.4. Morphology and Composition analysis

The morphological aspects of deposited SnS thin films of various thicknesses were recorded using FE-SEM and are displayed in figures 4(a)–(d). The grain morphologies are distinct from the results that had reported earlier for thermally evaporated thin films at room temperature and also elevated substrate temperature Threadworm-like grains are uniformly distributed over the surface. The sizes of the grains exhibit random orientation as it varies from one to another, which is in the range 700nm.

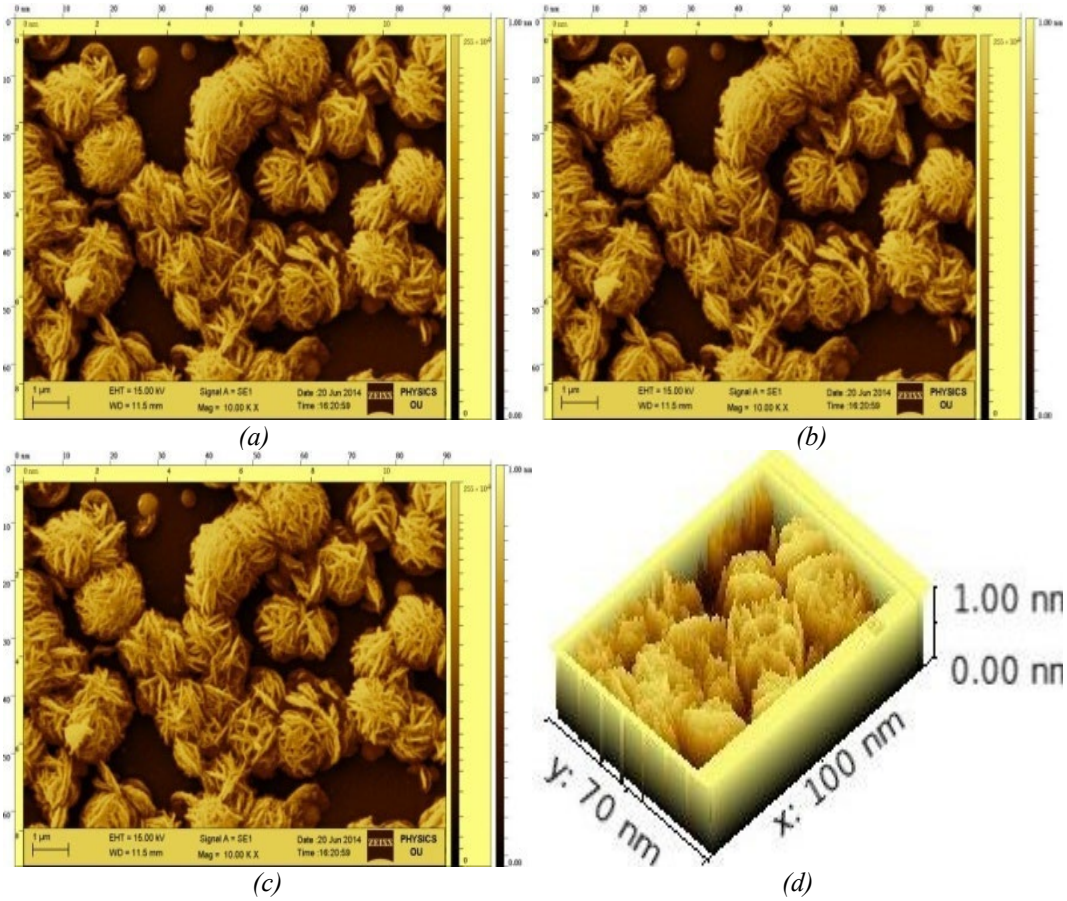

Fig.3.FESEM images of SnS thin film of thickness(a) 500nm(b)550nm(c)600nm(d)650nm(d)700nm.

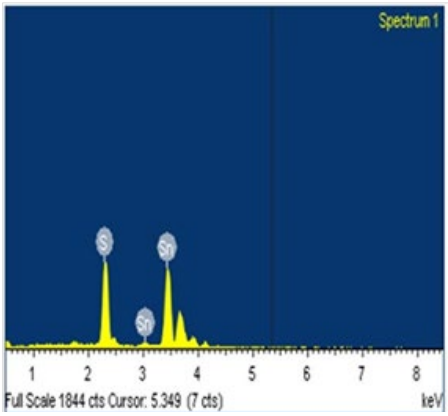

Different Film thickness (nm)	Sn/S (Atomic percentage)	
	Sn	S
500	50.05	49.95
550	50.35	49.65
600	50.47	49.53
650	50.65	49.35
700	50.76	49.24

Fig.4.EDS spectra of SnS thin films at different thicknesses (500nm–700nm).

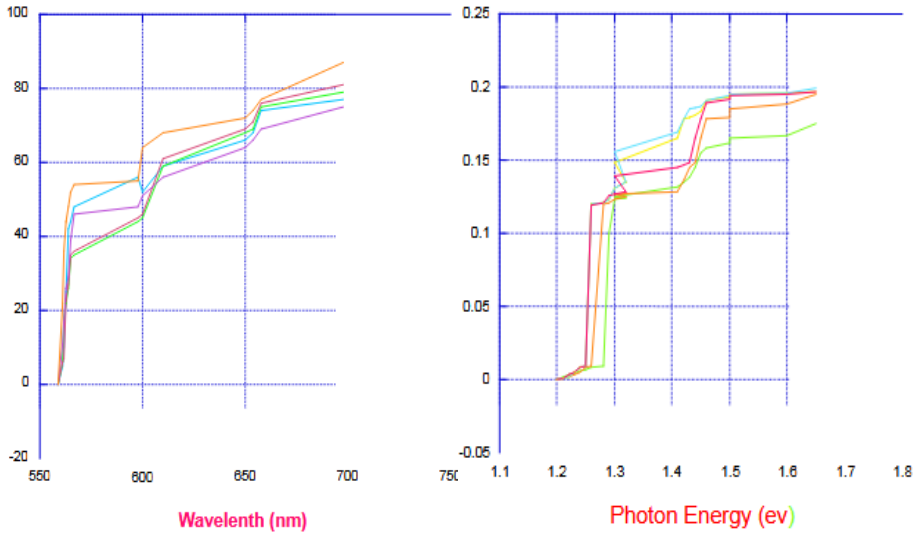

Fig. 6.Optical transmittance spectra, (b)$(\alpha hv)^2$versus photon energy (hv) plot of SnS thin films of different thicknesses.

Further, to study elemental composition, figure 4shows EDX analysis was performed for all the prepared SnS thin film samples. Irrespective of the thickness, all the films were stoichiometric with Sn to S atomic percent ratio~1.In contrast, for the SnS thin films deposited at constant substrate temperatures, stoichiometry depends on the thickness [27]. Hegde *et al* [25] reported that the sulfur-rich SnS film grown at lower substrate temperatures (50°C–200°C)with the occurrence of additional phases such as SnS_2 and Sn_2S_3,however,the film prepared at 300°C had shown balanced stoichiometry as well as single-phase SnS devoid of any secondary phases.

3.5. Photo detector characteristics

To evaluate the film thickness effect on the photoresponse properties ,thin-film photo detectors of SnS had been fabricated with a 1 mm active area. Ag contacts were made on SnS thin films with aid of a metal mask to investigate photoresponse under dark as well as538nm illumination with various power densities.Figures7(a) depicts the I–V(current &voltage)characteristics of the fabricated photo detector under light OFF and On conditions. The semi-log scale of the I-V curve s is plotted to depict the difference in photo current and dark current. When the applied voltage increases, the dark current increase progressively implying an Ohmic contact between Ag electrodes and SnS thin films. It is observed from the figures that in all the samples photo current values are far higher than the dark current due to increased photo generated carriers upon incident light. The predominant origin of photocurrent is due to the electron-hole pair generation during the illumination of semiconductors with energy equal to or greater than the bandgap energy.

The photocurrent (I_{PC}) is determined using $I_{PC}=I_{light}-I_{dark}$, where ,$I_{light}$ represents the current when illuminated with the wavelength of 532nmwith 5mWcm^{-2}power density. The estimated photo current for 520nm film under 5V bias voltage is 4.7×10^{-7}Aan disincreased with the thickness of the film as shown in Figure 7. The highest photocurrent of 44.2×10^{-7} A is observed in the 710 nm thin film sample can be attributed to increased crystallinity with fewer defects and hence reduced recombination of carriers.

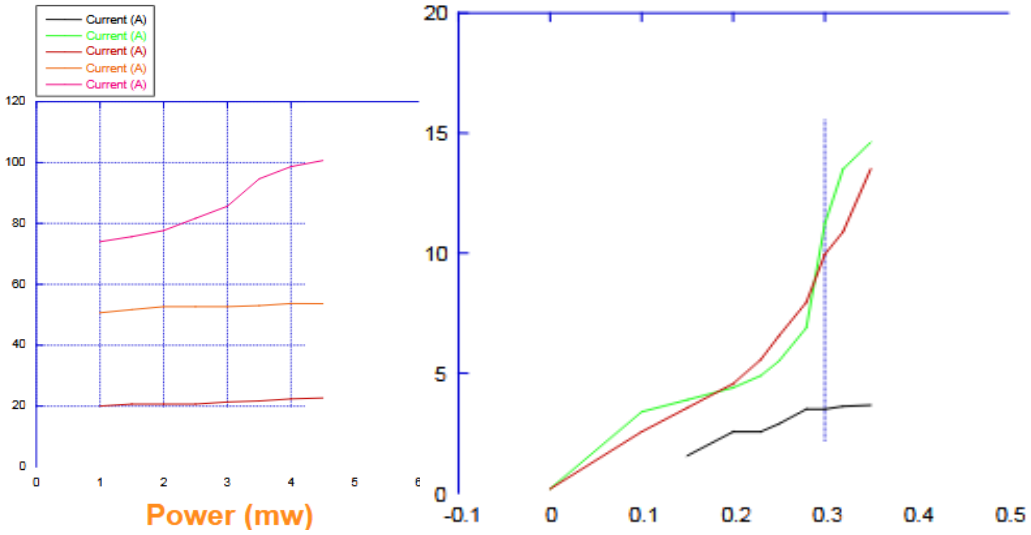

Fig. 7. I–V characteristics of the fabricated SnS thin film photo detectors o f different thickness under dark and illumination. (f) The variation of photocurrent with light intensity for SnS different thickness photo detectors.

Table 1. Estimated results for different film thickness

Film thickness(nm)	$R(AW^{-1})$	EQE(%)	D^*(Jones)	Risetime(s)	Falltime(s)
500	0.86×10^{-1}	24	5.12×10^{9}	5.4	5.3
550	1.38×10^{-1}	32	6.02×10^{9}	5.6	5.2
600	2.24×10^{-1}	54	8.82×10^{9}	5.4	5.2
650	7.72×10^{-1}	137	13.2×10^{9}	5.2	5.3
700	2.59×10^{-1}	51	6.30×10^{9}	5.4	5.2

The estimated results were given in table1.From the table, the values suggest that the sample with a thickness of 700 nm shows the least rise time compared to the fabricated devices indicating better photo response. This might be because of an increase in the drift movement of charge carriers there by reducing transit time. Because of the electron replenishment mechanism, which keeps the generated photocurrent flowing for the duration of the electron's life time, photo conductive-type detectors have a far slower response time than photo diode detectors. However, they fulfill broadband light detection requirements [1].

4. Conclusions

In summary, visible light photo detectors are fabricated using SnS thin films by thermal evaporation at room temperature. SnS thin films of different thicknesses varying from 500 nm to 700 nm are used to fabricate photo detectors to investigate the influence of thickness on photo detector performance. The prepared SnS thin films were of pristine SnS phase, stoichiometric, and free from SnS_2 and Sn_2S_3 impurity phases as confirmed by XRD, and Raman analysis. The structural characterization shows samples having orthorhombic structure and an increase in crystallinity with a thickness up to 700 nm. Morphological analysis of SnS thin films displayed that the films exhibit columnar plate-like grain morphology with different widths and thicknesses. The optical studies revealed high absorption for the thin film of a thickness of 680nm and an appropriate direct optical bandgap of 1.47eVfor maximum absorption of the visible light

Spectrum. The I–V characteristics of the fabricated photo detector under dark and illumination conditions indicated an increase in photocurrent with the thickness and highest photocurrent of 44.2×10^{-7} A is observed in the 710 nm sample.

Acknowledgments

The basic research was supported by JNTUH. The SEM, XRD and EDX, Hall measurement system analysis of samples is facilitated by OU and HCU Universities

References

[1] Krishnamurthi V et al., Adv. Mater. 32, 2004247 (2020).
[2] Dittrich H et al., Phys. Status Solidi A 206, 1034 (2009); https://doi.org/10.1002/pssa.200881242
[3] Zhou X et al., J. Mater. Chem. C 4, 2111 (2016).
[4] Tian H et al., Appl. Surf. Sci. 487, 1043 (2019); https://doi.org/10.1016/j.apsusc.2019.05.175
[5] Rahul K Y et al., Curr. Appl Phys. 31, 232 (2021).
[6] Calderon V H et al., ACS Appl. Energy Mater. 3, 6815 (2020).
[7] Schedel C et al., ACS Appl. Mater. Interfaces 13, 47954 (2021); https://doi.org/10.1021/acsami.1c13581
[8] Jang H et al., Adv. Funct. Mater. 31, 2006788 (2020).
[9] Devi N M et al., Semicond. Sci. Technol. 36, 025013 (2021); https://doi.org/10.1088/1361-6641/abcee1
[10] Shkir M et al., Sens. Actuators A 306, 111952 (2020); https://doi.org/10.1016/j.sna.2020.111952
[11] Kumara M et al., Nanoscale 9, 19201 (2017); https://doi.org/10.1039/C7NR07120E
[12] Khanzode P M et al., Optik 226, 165933 (2021); https://doi.org/10.1016/j.ijleo.2020.165933
[13] Hegde S S et al., Thin Solid Films 545, 543 (2013); https://doi.org/10.1016/j.tsf.2013.08.078
[14] Baby B H and Mohan D B, Sol. Energy 194, 61 (2019); https://doi.org/10.1016/j.solener.2019.10.049
[15] Hegde S S et al., Phys. B Condens. Matter. 406, 1143 (2011); https://doi.org/10.1016/j.physb.2010.12.068
[16] Hegde S S et al., Surf. Interfaces 10, 78 (2018); https://doi.org/10.1016/j.surfin.2017.12.003
[17] Cho J Y et al., J. Mater. Chem. A 8, 20206658 (2020).
[18] Johnson J B et al., Semicond. Sci. Technol. 14, 501 (1999); https://doi.org/10.1088/0268-1242/14/6/303
[19] Qin Y et al., Phys. Status Solidi A 218, 2000642 (2021); https://doi.org/10.1002/pssa.202000642
[20] Hegde S S et al., Chem. Phys. Lett. 54, 137665 (2020); https://doi.org/10.1016/j.cplett.2020.137665
[21] Shan Y et al., Adv. Funct. Mater. 30, 2001298 (2020); https://doi.org/10.1002/adfm.202070134
[22] Sinsermsuksakul S et al., Adv. Energy Mater. 4, 1400496 (2014); https://doi.org/10.1002/aenm.201400496
[23] Reddy T S et al., RSC Adv. 6, 95680 (2016); https://doi.org/10.1039/C6RA20129F
[24] Mahdi M S et al., J. Alloys Comp. 735, 2256 (2018); https://doi.org/10.1016/j.jallcom.2017.10.203
[25] Balakarthikeyan R et al., Optik 244, 167460 (2021); https://doi.org/10.1016/j.ijleo.2021.167460

[26] Yuan S et al., AIP Adv. 9, 095205 (2019).
[27] Krishna H M et al., Sol. Energy 221, 412 (2021);
https://doi.org/10.1016/j.solener.2021.04.061